

Use of micro-PIXE for elemental characterization and iron uptake evaluation in zebrafish larvae exposed to iron oxide nanoparticles

M.R. Caloni^{a,*}, E.M.N. Oliveira^{a,b}, D. de V. Bauer^c, M.R. Vianna^b, J.F. Dias^c, R.M. Papaléo^a

^a Interdisciplinary Center of Nanoscience and Micro-Nanotechnology, Pontifical Catholic University of Rio Grande do Sul, Av. Ipiranga 6681, Porto Alegre, Brazil

^b Laboratory of Developmental Biology of the Nervous System, School of Sciences, Pontifical Catholic University of Rio Grande do Sul, Av. Ipiranga 6681, Porto Alegre, Brazil

^c Ion Implantation Laboratory, Institute of Physics, Federal University of Rio Grande do Sul, Av. Bento Gonçalves 9500, Porto Alegre, Brazil

ARTICLE INFO

Keywords:

PIXE
Nanotoxicology
Zebrafish
Iron oxide nanoparticles

ABSTRACT

We report on the evaluation of iron content and biodistribution in zebrafish larvae (*Danio rerio*) exposed to dextran-coated superparamagnetic iron oxide nanoparticles (SPION-DX) using the micro-PIXE technique. We compare results of elemental 2D maps and Fe quantification obtained from two different sample preparation procedures: one using sagittal slices prepared by cryo-sectioning and another using entire dehydrated larvae. Independently of the preparation method used, the Fe content in the tissues of exposed animals is significantly higher than in the controls, but the increase is not proportional to the exposure level. In addition, 2D elemental maps show a somewhat homogeneous Fe distribution in the larvae, with some samples showing a slight enhancement in Fe content near the gut. From the PIXE data a curve correlating the exposure (nanoparticle concentration in the fish water) to the iron content in the body was obtained, which shows a saturation trend towards high exposure doses.

1. Introduction

Magnetic nanoparticles have been increasingly used in biological contexts due to their unique physicochemical properties, which allow a wide range of *in vivo* therapeutic and diagnostic applications [1,2]. Among the different magnetic nanoparticles, superparamagnetic iron oxides (SPIONs) are one of the most prevalent in biomedical applications [3,4]. For example, they are very useful contrast agents for medical imaging [5,6], and may act as heating centers in magneto hyperthermia of tumors [7,8]. SPIONs consist of a magnetite or maghemite core with the surface modified by a stabilizing coating layer (usually biocompatible polymers), which may be further modified to add different functionalities to the system [9]. In spite of the biodegradability in the body of iron oxide nanoparticles and the relatively low levels of toxicity usually reported [10,11], there are still concerns related to their safe use in humans [12,13].

Zebrafish (*Danio rerio*) has often been used as a model organism for *in vivo* toxicological studies of nanomaterials [14–21]. There are several advantages of the model. Zebrafish rapidly incorporate chemical substances from the aqueous medium into tissues and the central nervous system. They have a large fecundity and rapid external development, which enable high throughput analysis. In addition, conserved

developmental mechanisms and the significant genomic similarity make experimental data, in principle, translational to humans [22,23]. One key element in toxicological studies is the actual accumulation in the tissues of the active compound, following exposure to a given amount in water. This is often an unknown parameter, and most investigations only take into consideration the amount of a given substance introduced in the water system to parameterize the toxicological effects.

In this work, we show preliminary results on the application of the micro-PIXE technique to investigate the effective iron incorporation into zebrafish larvae after exposure to iron oxide nanoparticles at concentrations up to 8 mM of Fe in water. The elemental distributions (2D maps) and Fe quantification obtained from different sample preparation procedures is compared and used to derive a curve correlating the exposure (nanoparticle concentration in the fish water) to the iron content in the body.

2. Materials and methods

2.1. Nanoparticle synthesis and characterization

Iron oxide nanoparticles were prepared by the coprecipitation

* Corresponding author.

E-mail address: matheus.caloni@acad.pucrs.br (M.R. Caloni).

<https://doi.org/10.1016/j.nimb.2019.09.035>

Received 7 May 2019; Received in revised form 19 September 2019; Accepted 23 September 2019

Available online 05 October 2019

0168-583X/© 2019 Elsevier B.V. All rights reserved.

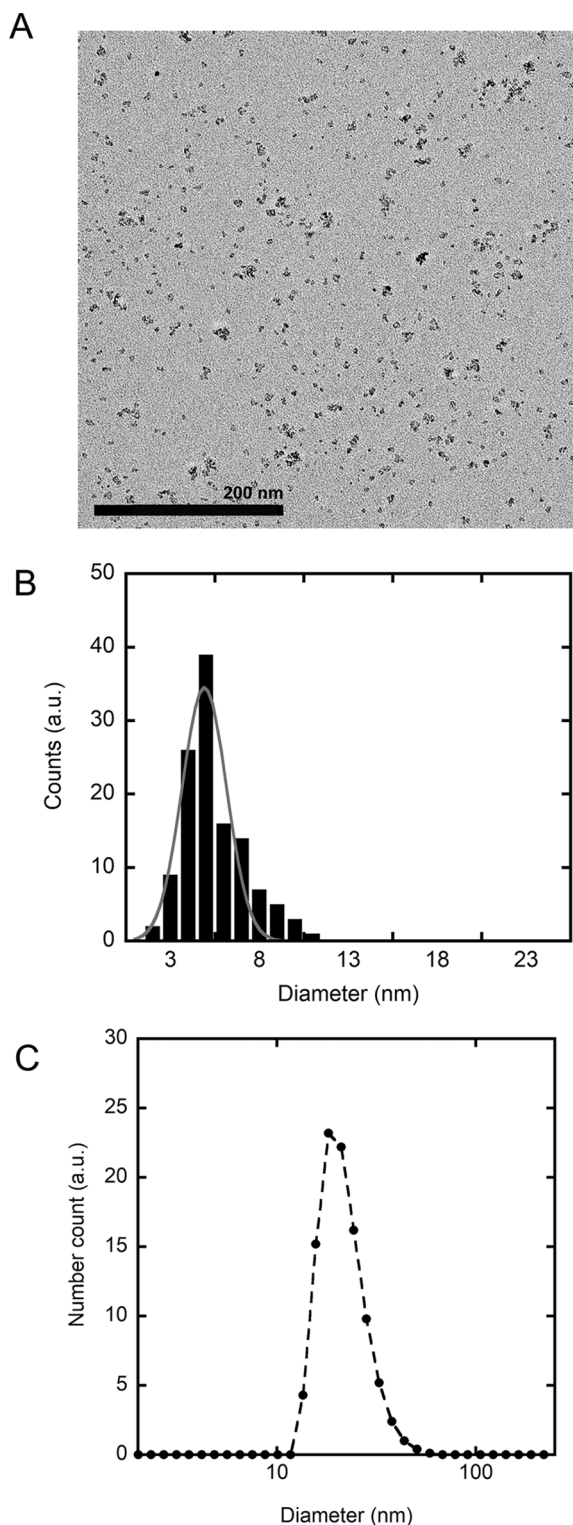


Fig. 1. Physical characteristics of the iron oxide nanoparticles. TEM micrograph of SPION-DX deposited on a formvar-coated Cu grid is shown in (A) and the corresponding size distribution in (B). The distribution of the nanoparticles hydrodynamic diameters in aqueous media (pH = 8.0) measured by light scattering is given in (C).

method in the presence of dextran (T10 - Pharmacosmos) as described in Ref. [24]. The remaining free dextran was removed from the nanoparticle dispersion by centrifugation at 3600 rpm for 30 min in Amicon tubes (cut off at 50 kDa – Millipore). Next, the dextran coating was

crosslinked using 35 mL of 5 M sodium hydroxide (Merck) and 14 mL of epichlorohydrin (Sigma-Aldrich), added to the nanoparticles solution and stirred overnight (approximately 14 h). In the final step, the dextran layer was aminated by reacting the compound with 60 mL of 28% ammonium hydroxide (Merck) under stirring for 24 h. Two additional purification steps were employed at the end of the synthesis: one to remove the excess of ammonium hydroxide by dialysis (MWCO 12–14 kDa – Millipore) and a final purification by centrifugation in Amicon tubes (MWCO 50 kDa – Millipore).

The morphology and size distribution of the nanoparticles were analyzed by transmission electron microscopy (TEM, JEM-2010 200 kV, JEOL) and by dynamic light scattering in a Zetasizer (Malvern). Before collecting the samples for microscopy (or for the exposure assays), the stock solution was sonicated at 40 kHz for 10 min and vortexed. Samples were then prepared by dripping a diluted solution of the nanoparticles on a TEM grid.

The resulting nanoparticles are of the *CLIO-NH₂* family (aminated crosslinked iron oxide nanoparticles) [25], with an iron oxide core of about 6 nm (as measured by TEM) and hydrodynamic radius in aqueous solutions of ~11 nm (see Fig. 1).

2.2. Zebrafish handling and exposure assay

Adult wild-type zebrafish animals (*Danio rerio*) of AB strain were maintained in an automated recirculating system (Tecniplast, Italy) under standard conditions for this species in the aqueous system ($28 \pm 2^\circ\text{C}$, conductivity of 500–800 μS , pH = 7.5 ± 0.5 equilibrated with Instant Ocean® salt, and photoperiod of 14:10 light/dark). Embryos were obtained by crossing females and males at a 1:2 proportion and viable embryos were selected 1-hour post-fertilization under a stereomicroscope [26].

The animals were exposed for a period of five days in a solution of SPION-DX, with iron concentrations of 2.0 and 8.0 mM, as measured by UV spectroscopy and ICP-MS. Fig. 2 provides a timeline of the exposure protocol. Embryos were kept in 24-well cell culture dishes with 4 embryos per well in a BOD incubator with controlled temperature and humidity. The water in which animals were kept (including the nanoparticles) was changed daily until the end of the experiment. The iron concentration of the replaced volumes from each exposure day was quantified by ICP-MS, and no significant variation was observed among samples. All experiments and handling procedures were approved by the Institutional Animal Care Committee (CEUA-PUCRS, number 7127), following the guidelines of the Canadian Council on Animal Care (CCAC) [27] for use of fish in research, and of the Brazilian legislation (No. 11.794/08).

2.3. Sample preparation for micro-PIXE analysis

Samples for micro-PIXE analysis were prepared using either sliced or whole-body larvae. Sliced samples were produced by cryo-sectioning at a sagittal orientation. Compared to standard histological protocols such as paraffin-embedding, cryo-sectioning does not require a series of chemical dehydration and washings with strong solvents that could introduce contaminants to the sample, and requires the least number of steps for sample preparation. Following cryo-euthanasia, the larvae were fixed in NBF 10 for 24 h, at room temperature, which was evaluated as the optimal fixation protocol for zebrafish larvae [28]. After fixation, the larvae were rinsed three times in deionized water and cut in a cryostat microtome (Leica Biosystems®). 60 μm sections were laid onto Mylar® substrates and dehydrated in an evacuated desiccator at room temperature. To prepare whole-body samples, animals were also sacrificed using cryo-euthanasia, and subsequently the larvae were dehydrated overnight in ethanol 70% at room temperature. After that, the whole bodies were laid onto a carbon substrate.

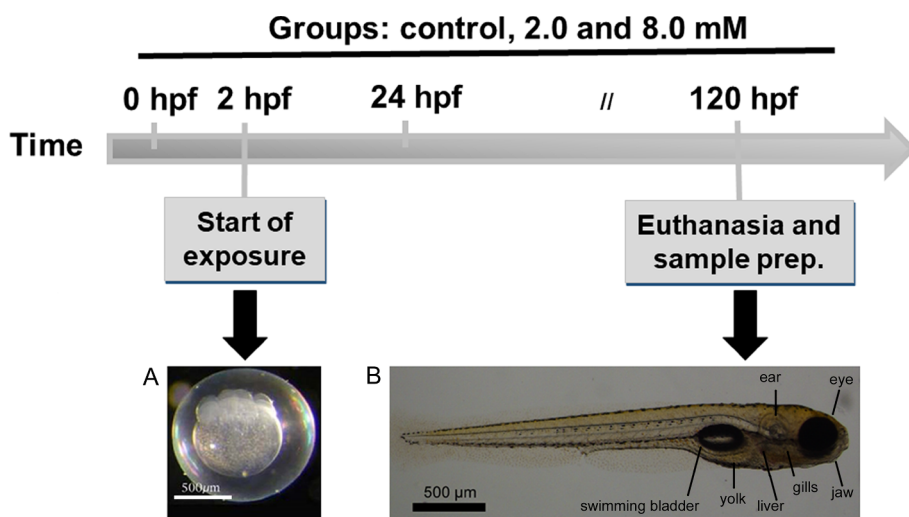


Fig. 2. Timeline of the exposure protocol. Zebrafish embryos were exposed to nanoparticle dispersions containing 2.0 and 8.0 mM of Fe at 2 h post-fertilization. Each day the medium containing the nanoparticles was changed by a fresh aliquot of nanoparticle solution. The exposure ended 5 days post-fertilization, when the animals were euthanised and fixed for micro-PIXE analysis.

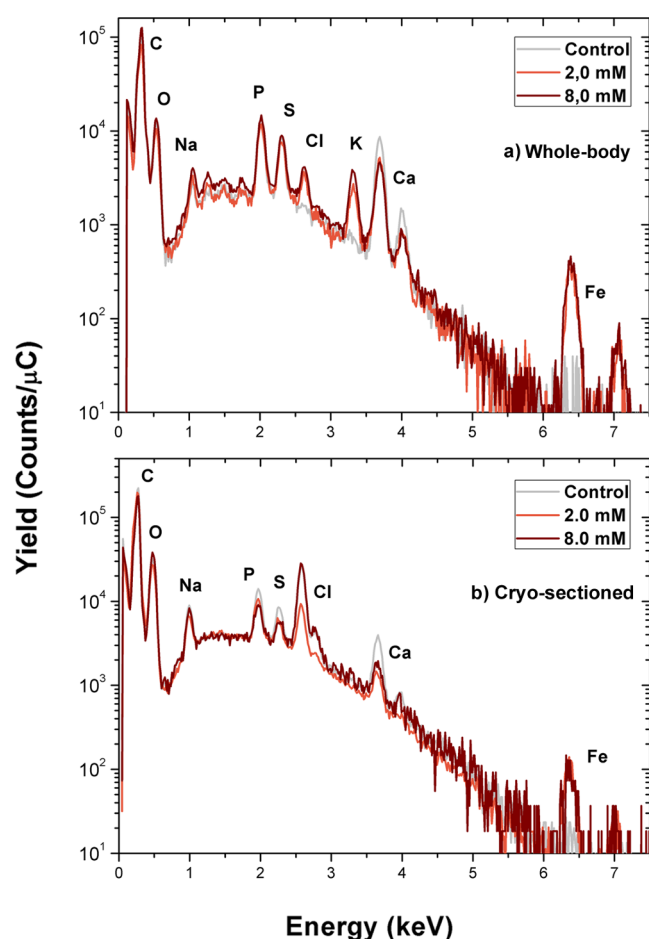


Fig. 3. Averaged PIXE spectra of zebrafish larvae exposed to 2.0 and 8.0 mM of SPION-DX for 5 days and prepared as (a) whole-body or (b) 60 μm -thick cryo-sections. Spectra from control samples were also added in the figure.

2.4. micro-PIXE measurements and data analysis

Micro-beam Particle Induced X-ray Emission (micro-PIXE) analysis was carried out at the 3-MV Tandem accelerator of the Ion Implantation Laboratory (Federal University of Rio Grande do Sul, Brazil) using a 3 MeV proton beam with an average spot size of $6.25 \mu\text{m}^2$ and mean current of 70 pA. The charge was collected on the target holder which is calibrated against a Faraday cup positioned behind the target in the

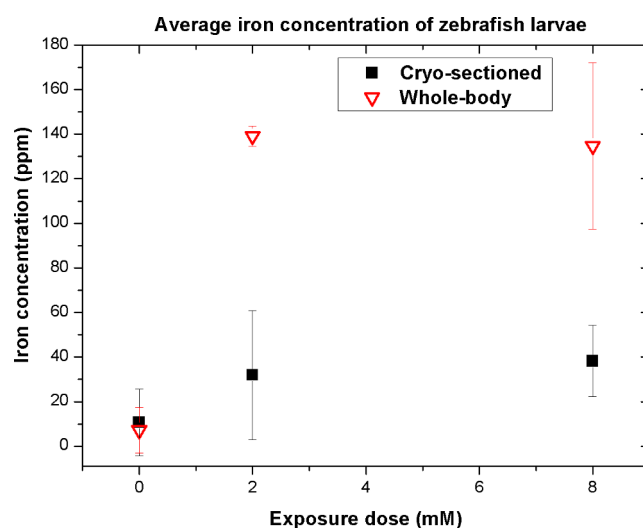


Fig. 4. Iron concentration in zebrafish larvae treated with SPION-DX at different exposures. Squares are data obtained from cryo-sectioned and triangles from whole-body samples. The interrogation depth of the proton beam ($\sim 100 \mu\text{m}$) is larger than the slice thickness ($\sim 60 \mu\text{m}$), but smaller than the thickness of the whole-body sample. The data is shown as the mean \pm the standard error (estimated by GUPIXWIN[®]).

direction of the incident beam. The target holder is electrically insulated from the rest of the reaction chamber. For thin samples where the proton beam is transmitted through, the total charge is the sum of both measurements. Micro-PIXE experiments were performed using the Oxford Microbeams[®] system, operating in the triplet mode. A scan size of $1000 \times 1000 \mu\text{m}^2$ was employed, which fitted the entire larvae's body. X-rays were recorded by a Sirius SDD (silicon drift detector) with a 140.5 eV energy resolution at 5.9 keV. This detector was placed at 135° with respect to the beam direction. Since this detector has a thin polymer window for the detection of light elements like carbon and oxygen, the detector was placed relatively far from the sample, which prevents most backscattered protons from reaching the silicon crystal due to the small detection solid angle. In this geometry, the number of backscattered particles reaching the detector is negligible. However, the count rates are quite low, demanding long data acquisition times.

Measurements of iron content were performed in controls and animals exposed to 2 and 8 mM of SPIONs, keeping the same acquisition time and scanning area size. In the case of cryo-sectioned samples, 3 different animals per concentration were analyzed (including the controls). For the whole-body samples, 2 larvae per concentration were analyzed.

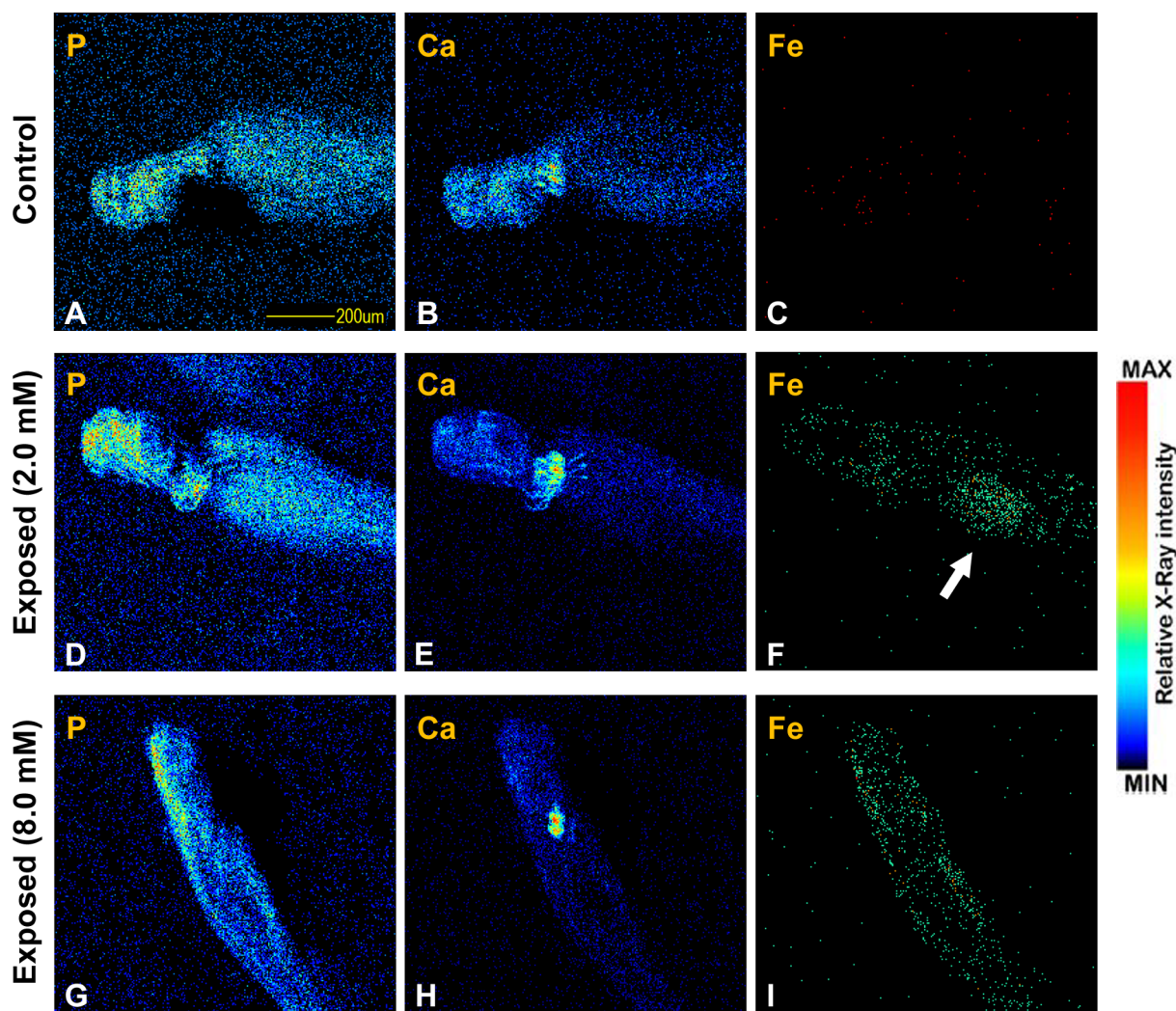


Fig. 5. Micro-PIXE elemental maps of phosphorus, calcium and iron obtained from dehydrated whole-body larvae: (A-C) control samples; (D-F) larvae exposed to 2.0 mM of SPION-DX for 5 days; and (G-I) larvae exposed to 8.0 mM of SPION-DX for five days. The color scale used in this figure is the same for all maps. Fig. 2 provides anatomical information for the zebrafish from a sagittal view.

X-ray spectra were analyzed by the GUPIXWIN software developed in the University of Guelph (Canada) [29] in two different approaches. Spectra from sectioned larvae were processed in an intermediate width sample approximation, using a beam exit energy of 2.06 MeV, and matrix correction of 0.75 C, 0.15 O and 0.15 N, extracted from a RBS analysis of canned tuna fish [30]. We note that although the hydrogen content is not explicitly included in the matrix, H does not contribute neither to photon self-absorption nor to secondary fluorescence in the target. Thus, neglecting hydrogen in the matrix corrections has no effect in the absolute concentrations of iron calculated by GUPIXWIN. The same matrix correction was performed for whole-body larvae but applying the thick sample approximation. In this case, 3 MeV protons penetrate about 100 μm in the soft tissue. For 6.4 keV X-rays from Fe, it is estimated that about 16% of the X-rays emitted from a depth of 100 μm will be absorbed by the tissue. However, it is important to stress that effects like secondary fluorescence and X-ray absorption in the target are fully accounted for by the GUPIXWIN software. Finally, the standardization of the micro-PIXE system was carried out with X-ray standards from Micromatter® (SiO, Mn, CuSx and GaP).

3. Results and discussion

The main elements present in the untreated zebrafish larvae as seen by PIXE are C, O, P, S, Ca, and Na. This is presented in Fig. 3 where

averaged micro-PIXE spectra obtained from both control and exposed animals are shown. Although the spectra obtained from control samples prepared by cryo-sectioning or by dehydration are similar, slight variations in elemental composition were observed depending on the sample preparation procedure. For example, whole-body control samples did not exhibit a chlorine peak (which is very clear on the cryo-sectioned samples), but the calcium signal, on the other hand, was more intense than in cryo-sectioned samples. In addition, a few weak peaks appeared in the spectral region between 1 and 2 keV (associated to trace amounts of Mg, Al, and Si), which are not seen in cryo-sections.

It is well known that sample preparation is critical for the chemical integrity of biological samples. For example, formalin fixation of biological tissues can alter the elemental composition balance, especially of water-soluble ions such as P, S, Cl, and K [31]. Indeed, changes on the permeability of cell membrane may facilitate the leaching of elements [32]. In our case, an overall reduction of such peaks is observed in cryo-sectioned samples (which involves the use of formalin), consistent with the aforementioned observations. Also, Turnau et al [33] reported dislocation and major removal of K in chemically fixed *mycorrhiza* samples, when compared to freeze-dried specimens. This effect seems to be present also in the zebrafish larvae as potassium, an important trace element that actively participates in ionic homeostasis processes in zebrafish [34], was not observed in any of the controls. A more detailed investigation on the optimum sample preparation

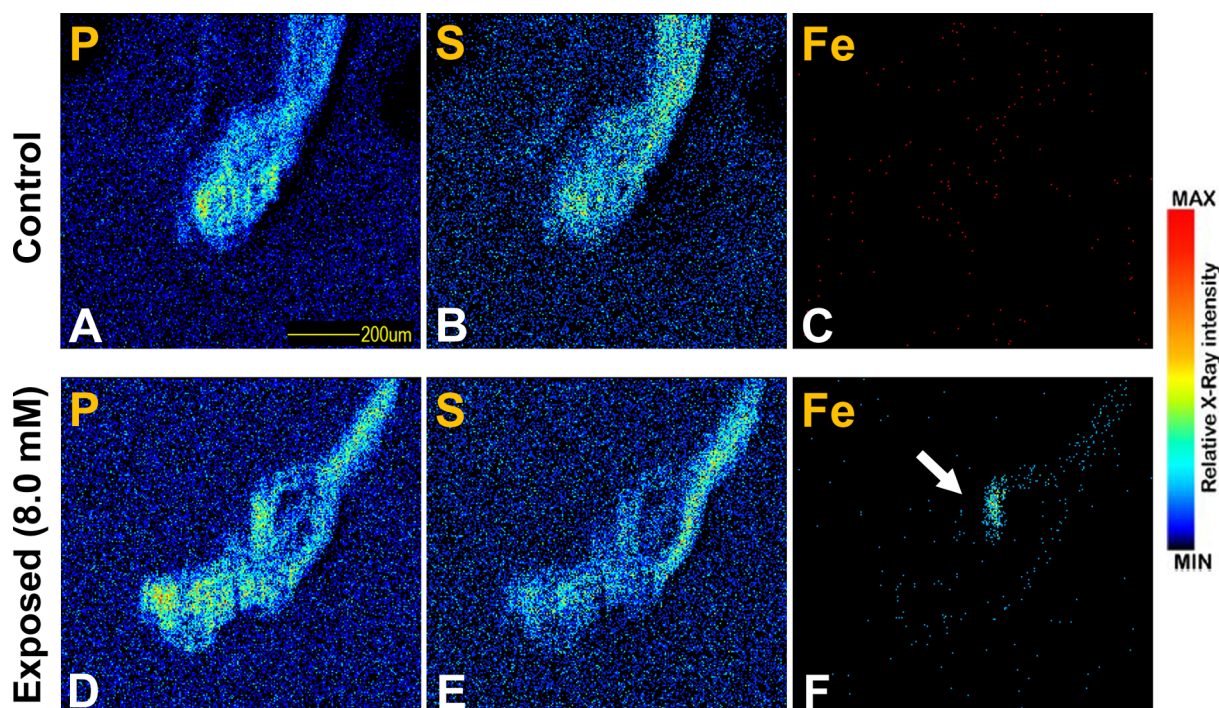


Fig. 6. Micro-PIXE elemental maps of phosphorus, sulfur, and iron present in zebrafish sagittal slices of (A–C) control samples and (D–F) samples exposed to 8.0 mM of SPION-DX.

procedure for zebrafish larvae is currently being evaluated in our laboratory and will be reported elsewhere.

The endogenous iron signal of control animals is very weak and close to the background in the micro-PIXE spectra (Fig. 3). Quantification of the absolute iron content in the samples indicates that less than 10 ppm of iron is present in the untreated larvae for both sample preparation procedures (Fig. 4). On the other hand, the iron signal is clearly detectable in the spectra of larvae exposed to the nanoparticles (Fig. 3). Thus, exposure to both concentrations of SPION-DX causes iron accumulation in the body and are detectable for both sample preparation procedures. The iron concentration of treated larvae reaches up to ~140 ppm in the whole-body samples, and only ~40 ppm in the slices. Interestingly, there is no important difference of iron uptake between larvae exposed to 2.0 and 8.0 mM of Fe, despite the fourfold increase in the exposure dose between the two cases (Fig. 4). For example, in whole-body samples, 139 ppm of iron was detected in a larva treated with 2.0 mM of Fe and 135 ppm in the 8.0 mM case exposure. In cryo-sectioned samples, the iron content of larvae exposed to a dose of 8.0 mM is slightly higher (40 ppm) compared to the ones exposed to 2.0 mM (30 ppm), although the variability lies within the uncertainty of the measurements. In any of the cases, a higher exposure dose does not cause an increase in the iron concentration of the larvae in the same proportion, suggesting a saturation of the physiological mechanisms of iron uptake at exposure levels beyond 2.0 mM. It is important to note that the substrates used in both sample preparations do not contribute significantly to the iron signal.

The differences observed in the total iron content seen in whole-body versus cryo-sectioned samples seem to arise from the contribution of the superficial layers, which are absent in the cryo-sectioned samples (apart from the slice edges). Since the larvae developed in water with suspended nanoparticles, the absorption of SPION-DX occurs necessarily through the epidermis and the gills. The mouth at such early stages is still undeveloped, and possibly do not work as a relevant pathway into the organism. Thus, although the interrogation depth of the proton beam is close to ~100 μm, the passive absorption through the surface of the animal may have a strong contribution to the signal in the case of the whole-body samples.

In the 2D elemental maps of whole-body samples (Fig. 5), iron is present in the entire extension of the larvae. However, in the case of cryo-section maps (Fig. 6), iron is distributed mostly around the gut region and to a smaller extent at the borders of the slice. This observation also supports nanoparticle uptake through the epidermis of the larva as an important pathway of Fe accumulation. Although the gills could be another mean to internalize nanoparticles, no important enhancement of the signal in this region was observed in any iron map. A slight enhancement of Fe accumulation was seen in the gut region of an animal exposed to 2.0 mM of Fe (Fig. 5f). Preferential Fe accumulation in the gut region was also detected in cryo-sections of exposed larvae (Fig. 6). This region contains structures such as the liver, swimming bladder and yolk sac. In humans, SPIONs are mainly absorbed by the reticuloendothelial system and the liver is considered as the main organ of accumulation [35], which may also be the case for zebrafish larvae.

Figs. 5 and 6 also show the spatial distribution of endogenous elements such as P, S, and Ca. Most of the endogenous elements are homogeneously distributed throughout the larvae, as seen in the P and S maps. However, calcium maps of whole-body specimens (exposed or controls) exhibit an enhancement near the head (Figs. 5b, e, and h). The source of such signal is yet unclear.

4. Conclusion

Micro-PIXE was applied to investigate uptake and biodistribution of Fe in developing zebrafish exposed to iron oxide nanoparticles dispersed in the aqueous system. Although some variations were seen in the spectra (and thus in the elemental composition) obtained from cryo-sectioned or whole-body samples, the data from the two methods of sample preparation were consistent, with an overall reduction in signal intensity observed in the cryo-sectioned samples. The Fe concentration in the tissues of exposed animals is higher when compared to those from control animals, but with an indication of uptake saturation at exposures close to 2 mM of Fe. Elemental maps of whole-body samples show that Fe is distributed throughout the entire larvae's superficial layers, demonstrating that the exposures provoke retention of SPION-

DX in the epidermal tissue. A slight enhancement in the gut region of a cryo-sectioned sample may be related to preferential accumulation sites of SPION-DX in internal structures such as liver and yolk sac.

Here we show preliminary data on elemental maps of zebrafish larvae exposed to nanoparticles investigated in a yet limited number of animals by micro-PIXE. The successful use of the technique to obtain information of accumulation and spatial distribution of elements localized to specific organs and tissues at exposure conditions typical of toxicological investigations calls for additional systematic measurements. Work is currently in progress in our laboratory to produce an expanded set of data, aiming to identify the most suitable and reliable sample preparation protocol, and to establish a complete curve correlating a broad range of exposure doses with the iron accumulation and distribution in the larvae.

Acknowledgements

This work has been partially funded by the research networks of the *National Institute of Surface Engineering* (INCT, CNPq/CAPES) and *Synthesis and Characterization of Nanostructured Materials by Ion Beams* (PRONEX, CNPq/FAPERGS). M.R.C. also acknowledges CAPES for a scholarship. E.M.N. is supported by CNPq (409421/2017-0). M. R. V. has a CNPq fellowship (308404/2015-7) and is funded by CNPq (425818/2018-7).

References

- [1] A.H. Lu, E.L. Salabas, F. Schüth, Magnetic nanoparticles: synthesis, protection, functionalization, and application, *Angew. Chem. - Int. Ed.* 46 (2007) 1222–1244, <https://doi.org/10.1002/anie.200602866>.
- [2] A.S. Teja, P.Y. Koh, Synthesis, properties, and applications of magnetic iron oxide nanoparticles, *Prog. Cryst. Growth Charact. Mater.* 55 (2009) 22–45, <https://doi.org/10.1016/j.pcrysgrow.2008.08.003>.
- [3] A.K. Gupta, M. Gupta, Synthesis and surface engineering of iron oxide nanoparticles for biomedical applications, *Biomaterials* 26 (2005) 3995–4021, <https://doi.org/10.1016/j.biomaterials.2004.10.012>.
- [4] A. Ito, M. Shinkai, H. Honda, T. Kobayashi, Medical application of functionalized magnetic nanoparticles, *J. Biosci. Bioeng.* 100 (2005) 1–11, <https://doi.org/10.1263/jbb.100.1>.
- [5] R.Y. Hong, B. Feng, L.L. Chen, G.H. Liu, H.Z. Li, Y. Zheng, D.G. Wei, Synthesis, characterization and MRI application of dextran-coated Fe₃O₄ magnetic nanoparticles, *Biochem. Eng. J.* 42 (2008) 290–300, <https://doi.org/10.1016/j.bej.2008.07.009>.
- [6] S. Laurent, D. Forge, M. Port, A. Roch, C. Robic, Elst L. Vander, R.N. Muller, Magnetic iron oxide nanoparticles: synthesis, stabilization, vectorization, physico-chemical characterizations and biological applications, *Chem. Rev.* 108 (2008) 2064–2110, <https://doi.org/10.1021/cr068445e>.
- [7] M. Bañobre-López, A. Teijeiro, J. Rivas, Magnetic nanoparticle-based hyperthermia for cancer treatment, *Reports Pract. Oncol. Radiother.* 18 (2013) 397–400, <https://doi.org/10.1016/j.rpor.2013.09.011>.
- [8] R. Avazzadeh, E. Vashghani-Farahani, M. Soleimani, S. Amanpour, M. Sadeghi, Synthesis and application of magnetite dextran-spermine nanoparticles in breast cancer hyperthermia, *Prog. Biomater.* 6 (2017) 75–84, <https://doi.org/10.1007/s40204-017-0068-8>.
- [9] T.D. Schladt, K. Schneider, H. Schild, W. Tremel, Synthesis and bio-functionalization of magnetic nanoparticles for medical diagnosis and treatment, *Dalton Trans.* 40 (2011) 6315–6343, <https://doi.org/10.1039/c0dt00689k>.
- [10] K.T. Geiss, J.M. Gearhart, J.J. Schlager, S.M. Hussain, K.L. Hess, In vitro toxicity of nanoparticles in BRL 3A rat liver cells, *Toxicol. Vitro* 19 (2005) 975–983, <https://doi.org/10.1016/j.tiv.2005.06.034>.
- [11] S.J.H. Soenen, U. Himmelreich, N. Nuytten, M. De Cuyper, Cytotoxic effects of iron oxide nanoparticles and implications for safety in cell labelling, *Biomaterials* 32 (2011) 195–205, <https://doi.org/10.1016/j.biomaterials.2010.08.075>.
- [12] B. Kong, J.H. Seog, L.M. Graham, S.B. Lee, Experimental considerations on the cytotoxicity of nanoparticles, *Nanomedicine* 6 (2011) 929–941, <https://doi.org/10.2217/nmm.11.77>.
- [13] A. Liskova, M. Kuricova, B. Smolkova, M. Dusinska, J. Tulinska, N. El Yamani, E. Rollerova, E. Rundén-Pran, Immunotoxicity, genotoxicity and epigenetic toxicity of nanomaterials: new strategies for toxicity testing? *Food Chem. Toxicol.* 109 (2017) 797–811, <https://doi.org/10.1016/j.fct.2017.08.030>.
- [14] G.M.T. de Oliveira, E.M.N. de Oliveira, T.C.B. Pereira, R.M. Papaléo, M.R. Bogo, Implications of exposure to dextran-coated and uncoated iron oxide nanoparticles to developmental toxicity in zebrafish, *J. Nanopart. Res.* 19 (2017), <https://doi.org/10.1007/s11051-017-4074-5>.
- [15] G.M.T. De Oliveira, L.W. Kist, T.C.B. Pereira, J.W. Bortolotto, F.L. Paquete, E.M.N. De Oliveira, C.E. Leite, C.D. Bonan, N.R. De Souza Basso, R.M. Papaléo, M.R. Bogo, Transient modulation of acetylcholinesterase activity caused by exposure to dextran-coated iron oxide nanoparticles in brain of adult zebrafish, *Comp. Biochem. Physiol. Part - C Toxicol. Pharmacol.* 162 (2014) 77–84, <https://doi.org/10.1016/j.cbpc.2014.03.010>.
- [16] X. Zhu, S. Tian, Z. Cai, Toxicity assessment of iron oxide nanoparticles in zebrafish (Danio rerio) early life stages, *PLoS One* 7 (2012) 1–6, <https://doi.org/10.1371/journal.pone.0046286>.
- [17] A.P. Fifi, G. Radaelli, E. Bonaiuto, G. Chemello, I. Olivotto, M. Magro, F. Maradonna, F. Gigliotti, F. Vianello, C. Piccinetti, B. Randazzo, O. Carnevali, Oxytetracycline delivery in adult female zebrafish by iron oxide nanoparticles, *Zebrafish* 13 (2016) 495–503, <https://doi.org/10.1089/zeb.2016.1302>.
- [18] P.V. Asharani, Y. Lianwu, Z. Gong, S. Valiyaveetil, Comparison of the toxicity of silver, gold and platinum nanoparticles in developing zebrafish embryos, *Nanotoxicology* 5 (2011) 43–54, <https://doi.org/10.3109/17435390.2010.489207>.
- [19] S.M. Samaee, S. Rabbani, B. Jovanović, M.R. Mohajeri-Tehrani, V. Haghpanah, Efficacy of the hatching event in assessing the embryo toxicity of the nano-sized TiO₂ particles in zebrafish: a comparison between two different classes of hatching-derived variables, *Ecotoxicol. Environ. Saf.* 116 (2015) 121–128, <https://doi.org/10.1016/j.ecoenv.2015.03.012>.
- [20] D.P. Karunararatne, K.N. Wallace, M.K. Prochaska, S. Andreescu, X. Liu, E. Dumitrescu, Developmental toxicity of glycine-coated silica nanoparticles in embryonic zebrafish, *Environ. Pollut.* 229 (2017) 439–447, <https://doi.org/10.1016/j.envpol.2017.06.016>.
- [21] T.H. Chen, C.C. Lin, P.J. Meng, Zinc oxide nanoparticles alter hatching and larval locomotor activity in zebrafish (Danio rerio), *J. Hazard. Mater.* 277 (2014) 134–140, <https://doi.org/10.1016/j.jhazmat.2013.12.030>.
- [22] A.J. Hill, H. Teraoka, W. Heideman, R.E. Peterson, Zebrafish as a model vertebrate for investigating chemical toxicity, *Toxicol. Sci.* 86 (2005) 6–19, <https://doi.org/10.1093/toxsci/kfi110>.
- [23] G. Kari, U. Rodeck, A.P. Dicker, Zebrafish: an emerging model system for human disease and drug discovery, *Clin. Pharmacol. Ther.* 82 (2007) 70–80, <https://doi.org/10.1038/sj.cpt.6100223>.
- [24] N.R.S.B.M.L.Z., R.M.P. Elisa M. N. de Oliveira, Maximiliano S. da Rocha Ana Paula P. Froner, *Artigo, Quim. Nov.* 42 (2019) 57–64.
- [25] P. Wunderbaldinger, L. Josephson, R. Weissleder, Crosslinked iron oxides (CLIO): a new platform for the development of targeted MR contrast agents, *Acad. Radiol.* 9 (2002) 304–306, [https://doi.org/10.1016/S1076-6332\(03\)80210-6](https://doi.org/10.1016/S1076-6332(03)80210-6).
- [26] M. Westerfield, ZFIN: Zebrafish Book: Contents, Zebrafish Book. A Guid. Lab. Use Zebrafish (Danio rerio). 4th Ed., Univ. Oregon Press. Eugene. (n.d.).
- [27] Canadian Council on Animal Care guidelines on the care and use of fish in research, teaching and testing, *Can. Counc. Anim. Care.* (2005) 1–94.
- [28] J.E. Copper, L.R. Budgeon, C.A. Foutz, D.B. van Rossum, D.J. Vanselow, M.J. Hubley, D.P. Clark, D.T. Mandrell, K.C. Cheng, Comparative analysis of fixation and embedding techniques for optimized histological preparation of zebrafish, *Comp. Biochem. Physiol. Part - C Toxicol. Pharmacol.* 208 (2018) 38–46, <https://doi.org/10.1016/j.cbpc.2017.11.003>.
- [29] J.L. Campbell, N.I. Boyd, N. Grassi, P. Bonnick, J.A. Maxwell, The Guelph PIXE software package IV, *Nucl. Inst. Methods Phys. Res. B* 268 (2010) 3356–3363, <https://doi.org/10.1016/j.nimb.2010.07.012>.
- [30] L.A. Bouffleur, C.E.I. dos Santos, R. Debastiani, M.L. Yoneama, L. Amaral, J.F. Dias, Elemental characterization of Brazilian canned tuna fish using particle induced X-ray emission (PIXE), *J. Food Compos. Anal.* 30 (2013) 19–25, <https://doi.org/10.1016/j.jfca.2013.01.002>.
- [31] M.J. Hackett, J.A. Mcquillan, F. El-assaad, J.B. Aitken, A. Levina, D.D. Cohen, R. Siegle, E.A. Carter, G.E. Grau, H. Hunt, P.A. Lay, Chemical alterations to murine brain tissue induced by formalin fixation: implications for biospectroscopic imaging and mapping studies of disease, *Analyst* (2011) 2941–2952, <https://doi.org/10.1039/c0an00269k>.
- [32] A. Van Der Ent, W.J. Przybyłowicz, M.D. De Jonge, H.H. Harris, C.G. Ryan, G. Tylko, D.J. Paterson, A.D. Barnabas, P.M. Kopittke, J. Mesjasz-przybyłowicz, X-ray elemental mapping techniques for elucidating the ecophysiology of hyper-accumulator plants, *Tansley Review* (2018) 432–452, <https://doi.org/10.1111/nph.14810>.
- [33] K. Turnau, Heavy metal distribution in *Suillus luteus* mycorrhizas – as revealed by micro-PIXE analysis Heavy metal distribution in *Suillus luteus* mycorrhizas, *Nucl. Instrum. Methods Phys. Res. Sect. B* (2001), [https://doi.org/10.1016/S0168-583X\(01\)00631-0](https://doi.org/10.1016/S0168-583X(01)00631-0).
- [34] P. Hwang, M. Chou, Zebrafish as an animal model to study ion homeostasis, *Plügers Arch.* (2013) 1233–1247, <https://doi.org/10.1007/s00424-013-1269-1>.
- [35] A. Laskar, M. Ghosh, S.I. Khattak, W. Li, X.M. Yuan, Degradation of super-paramagnetic iron oxide nanoparticle-induced ferritin by lysosomal cathepsins and related immune response, *Nanomedicine* 7 (2012) 705–717, <https://doi.org/10.2217/nmm.11.148>.